

Integrating Thermal Sensors in a Microplate Format: Simultaneous
Real-Time Quantification of Cell Number and Metabolic Activity

Peer-reviewed author version

OUDEBROUCKX, Gilles; GOOSSENS, Juul; BORMANS, Seppe; VANDENRYT, Thijs; WAGNER, Patrick & THOELLEN, Ronald (2022) Integrating Thermal Sensors in a Microplate Format: Simultaneous Real-Time Quantification of Cell Number and Metabolic Activity. In: ACS Applied Materials & Interfaces, 14 (2), p. 2440-2451.

DOI: 10.1021/acsami.1c14668

Handle: <http://hdl.handle.net/1942/36467>

Integrating Thermal Sensors in a Microplate Format: Simultaneous Real-Time Quantification of Cell Number and Metabolic Activity

Gilles Oudebrouckx,^{*,†,‡,§} Juul Goossens,^{†,‡,§} Seppe Bormans,^{†,‡} Thijs Vandenryt,^{†,‡}
Patrick Wagner,[¶] and Ronald Thoelen^{*,†,‡}

[†]*Institute for Materials Research (IMO), Hasselt University, 3500 Hasselt, Belgium*

[‡]*IMEC vzw, Division IMOMECE, 3590 Diepenbeek, Belgium*

[¶]*Laboratory for Soft Matter and Biophysics, KU Leuven, 3001 Leuven, Belgium*

[§]*These authors contributed equally to this work*

E-mail: gilles.oudebrouckx@uhasselt.be; ronald.thoelen@uhasselt.be

Abstract

Microplates have become a standard tool in the pharmaceutical industry and academia for a broad range of screening assays. One of the most commonly performed assays is the cell proliferation assay, which is often used for the purpose of drug discovery. Microplate readers play a crucial role in this field, as they enable high-throughput testing of large sample numbers. Common drawbacks of the most popular plate reader technologies are that they are endpoint-based and most often require the use of detection reagents. As a solution, with this work, we aim to expand the possibilities of real-time and label-free monitoring of cell proliferation inside a microplate format by introducing

a novel thermal-based sensing approach. For this purpose, we have developed thin-film sensors that can easily be integrated into the bottom of standard 96-well plates. First, the accuracy and precision of the sensors for measuring temperature and thermal effusivity are assessed via characterization experiments. These experiments highlight the fast response of the sensors to changes in temperature and thermal effusivity, as well as the excellent reproducibility between different sensors. Later, proof-of-principle measurements were performed on the proliferation of *Saccharomyces cerevisiae*. The proliferation measurements show that the thermal sensors were able to simultaneously detect relative changes in cell number as well as changes in metabolic activity. This dual functionality makes the presented sensor technology a promising candidate for monitoring microplate assays.

Keywords: Thermal sensor, microplate reader, cell proliferation, cell number, metabolic activity

Introduction

Microplates have become a standard tool in industry and academia for practicing a broad range of screening assays. Some of the most commonly used assays are cell cytotoxicity and proliferation assays, which are crucial for research on drug discovery whereby the effect of certain compounds on the cells is assessed.¹ Microplate readers play an important role in this field, as they enable high-throughput analysis of large sample numbers. Currently, the most commonly used plate readers are optical-based, and therefore most often require a labeling or staining protocol.² Optical read-outs can be based on different principles including fluorescence intensity,^{3,4} luminescence⁵ or absorbance.⁶ Generally, these plate readers are limited to the use of endpoint assays, which merely provide one single snapshot view of the condition of the cell population.^{2,7} Therefore, endpoint microplate assays are not ideally suited to study biological questions with unknown timing and duration.

To facilitate and improve the study of unknown biological processes over time, real-

time plate reader technologies are desired. Currently, several real-time plate readers are commercially available. With the most popular solutions, the before-mentioned optical read-out technologies are integrated into environmentally controlled incubation chambers in which the microplate can be inserted.^{8,9} This way, a real-time optical read-out is possible under the desired environmental conditions.

A promising label-free alternative to real-time optical plate readers are electrical impedance-based plate readers.² Using micro-electronic sensors embedded in the bottom of the wells, electrical impedance data are registered continuously. Because of the difference in dielectric properties between the cells and the culture medium, changes in impedance will be measured during the proliferation process. These impedance measurements can be converted to a quantitative measure of cell number in real-time.^{7,10} In recent years, the functionality of this technology was demonstrated in numerous drug discovery studies.¹¹⁻¹⁴

Another label-free and real-time method for monitoring cell proliferation is isothermal microcalorimetry (IMC).¹⁵ Whereas impedance measurements are mainly used to track changes in cell number, IMC is used to monitor heat generated by the metabolic activity of the cell population. The metabolic activity can also be used as a measure of proliferation.^{16,17} By monitoring the metabolic response to specific compounds, this technique can serve in drug screening studies as well.¹⁸⁻²⁰ Since the year 2000, commercial instruments for performing IMC have significantly improved in terms of the required volume and the number of parallel measurements. For example, the SymCel calScreener™ (SymCel AB, Sweden) enables IMC measurements inside a 48-well plate format, however, individually sealed cups are required for each well.^{17,21}

With this work, we aim to expand the possibilities of label-free, continuous microplate monitoring by introducing a novel thermal-based sensing approach. We have developed thin-film sensors that can be easily integrated into the bottom of microplates. The design of the individual sensor structures is based on a Transient Plane Source (TPS) sensor (also called Hot Disk sensor).²²⁻²⁴ However, in this work, we adapted the sensor design to fit within

the well diameter of standard 96-well plates. Conventionally, the TPS-method is an ISO standard (ISO 22007) for the determination of thermal properties.²⁵ The method can be applied to a broad range of materials including solids,^{24,26–30} liquids,³¹ powders³² and thin films.^{33,34}

Within this work, the idea is to use similar sensors to monitor cell proliferation by continuously measuring changes in thermal properties that occur during the process. This principle is analogous to an electrical impedance-based read-out. However, here the principle relies on a difference in thermal properties between the cells and the culture media rather than on a difference in dielectric properties.³⁵ This idea has been demonstrated earlier in our work,^{36,37} and by others,³⁸ by measuring the thermal insulation effect at the sensor surface caused by a proliferating cell culture and biofilm formation. However, in these previous studies, experiments have been performed inside different types of sample tubes, while the presented study specifically aims to demonstrate that a thermal read-out can also be implemented into a standardized microplate format. Thermal-based sensing of cell number offers some advantages over impedance-based sensing. Impedance-based sensors can be susceptible to drift caused by electrochemical changes in the media.^{38,39} Furthermore, with impedance-based sensing, cells are exposed to electric fields which might damage cells or affect the activity of cell membrane channels.^{40–42} However, in this work we aim to present another advantage of thermal-based sensors over impedance-based sensors for monitoring cell proliferation by demonstrating additional functionality.

In addition to using thermal sensors for quantifying cell number during proliferation, we will assess whether these thermal sensing structures can simultaneously be used as temperature sensors. More specifically, we will investigate whether the temperature sensing is sufficiently sensitive to detect temperature changes caused by the metabolic heat of cells, as is done with IMC. Demonstrating this double functionality would imply that this single thermal-based system combines the functionality of both impedance-based and IMC sensor systems. Also in general, this type of accurate embedded sensors can provide a convenient

solution for the monitoring of the sample temperature during various experiments inside a microplate. For example, it is known that cell health and the cell proliferation process can significantly be affected by the incubation temperature.^{43–46} Consequently, accurate temperature monitoring can provide useful information.

Initially, various characterization experiments are performed to demonstrate the sensor’s ability to simultaneously measure thermal effusivity and temperature. Thereafter, via proof-of-principle experiments on the proliferation of *Saccharomyces cerevisiae* we demonstrate that, from measured changes in thermal insulation and temperature, it is possible to relatively quantify cell number and metabolic activity, respectively.

Working principle

Measuring thermal effusivity

As mentioned earlier, the design of the individual sensor structures is based on that of a TPS sensor. More specifically, since only a single-sided sample contact is made in this work, the presented sensor more closely resembles a Modified TPS (MTPS) sensor.³¹ A TPS sensor typically consists of a metal heating structure that is deposited on an electrically insulating polyimide foil substrate.^{22–24} Figure 1a shows a miniaturized version of such a sensor embedded at the bottom of a microplate well. During a conventional TPS measurement, a Joule heating current pulse is sourced through the metal structure (Figure 1b). As a result, the temperature of the metal structure itself will increase. This sensor temperature response can be measured directly by simultaneously measuring the voltage over the structure during the heating step via the 4-wire resistance measurement principle. The measured change in electrical resistance can be converted to temperature using equation (1). Thus, during measurement, the structure functions both as a heating element as well as a temperature sensor.

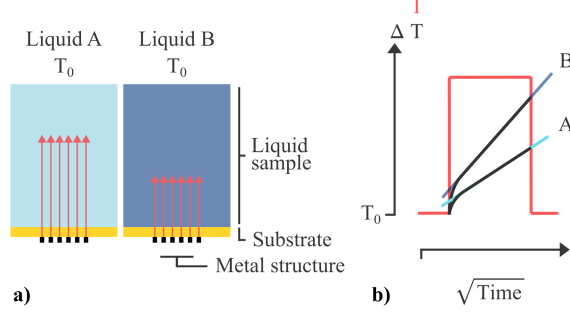


Figure 1: Conventional use of a TPS-sensor for measuring thermal effusivity (e). **(a)** Cross section of a TPS sensor measuring two liquids with different e ($e_B < e_A$). The heat generated by the metal structure is illustrated by red arrows. **(b)** The temperature response of the sensors to an identical heat pulse is visualized for both liquids. The higher slope of the temperature change of the metal structure for liquid B is due to the lower heat absorption of liquid B.

$$R = R_{ref}[1 + \alpha(T - T_{ref})] \quad (1)$$

where:

- R : Electrical resistance of structure [Ω]
- T : Temperature of structure [K]
- R_{ref} : Electrical resistance at temperature T_{ref} [Ω]
- α : Temperature coefficient of resistance [1/K]

When measuring homogeneous samples, as illustrated in Figure 1, the expected sensor temperature response can be described by equation (2).²³ Thus, by plotting the temperature response as a function of the square root of time, the response curve should approach a straight line (Figure 1b). Conventionally, the initial non-linear part at the start of the response curve, caused by the influence of the substrate, is ignored in data processing.²³ The slope (s) of the curve can be used as a measure of the thermal properties of the sample. More specifically, s is inversely proportional to the thermal effusivity (e), see equation (3), of the sample under test. The thermal effusivity can be described as the rate at which

a material can absorb heat. In the given example (Figure 1), liquid A has a higher e than liquid B. Therefore, liquid A is better able to absorb heat generated by the sensor structure. Consequently, the slope of the temperature response measured with liquid A is lower compared to the slope measured with liquid B.

$$\Delta T(t) = s\sqrt{t} \quad (2)$$

where:

T : Temperature [K]

s : Slope

t : Time [s]

$$e = \sqrt{\kappa\rho c_p} \quad (3)$$

where:

e : Thermal effusivity [$\text{Ws}^{1/2}/\text{m}^2\text{K}$]

κ : Thermal conductivity [W/mK]

ρ : Density [kg/m^3]

c_p : Specific heat capacity [J/kgK]

Measuring temperature

As described previously, the sensor structures are able to measure the absolute thermal effusivity (e) of a sample. In principle, the sensors can also be used to simply measure the temperature of the sample by using them as a Resistive Temperature Device (RTD).

For absolute temperature measurements, it is advised to use low measurement currents to minimize the self-heating effect.⁴⁷ However, we hypothesize that it is also possible to derive relative changes in sample temperature from the applied heating pulses. This idea is illustrated in Figure 2, where two identical liquids with different temperatures are present on the sensor. The time required to obtain the first data point at the start of the sensor temperature response curve (T_s) is not sufficient to probe beyond the boundaries of the substrate.²³ Therefore, it is expected that T_s is not influenced by the thermal properties of the sample. Consequently, T_s is only influenced by the sample temperature. As the sample temperature increases, T_s is expected to increase, and vice versa (Figure 2b). Whilst the thermal properties of most materials are temperature dependent, it is expected that limited changes in the sample temperature will not significantly affect measurements of e .⁴⁸ Therefore, in the illustrated example, the expected sensor temperature response curves have an identical slope at the end and thus are parallel. This hypothesis is validated in the experimental section.

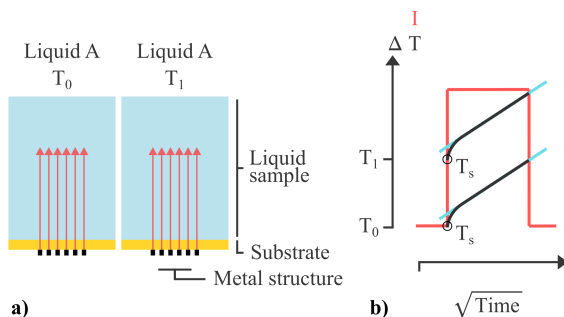


Figure 2: Use of sensors as RTD for measuring sample temperature during a measurement of thermal effusivity (e). **(a)** Two identical liquids are examined of which the liquid temperature differs ($T_1 > T_0$). **(b)** During a heating step, it is expected that the temperature difference between the liquids can be derived from the offset on the first data point at the start of the measured sensor temperature response (T_s).

Measuring cell proliferation.

As illustrated in Figure 3a, during cell proliferation, the number of cells at the sensor surface increases. In our previous work, we have already demonstrated that a continuous pulsed

thermal read-out can be used for the relative quantification of cell number in real-time.³⁷ As the cell number increases, the thermal insulation at the sensor surface increases. These changes in thermal properties can be derived from the measured slopes.³⁷ Thus, as the cell number increases, it is expected that the measured slope increases (Figure 3b). In the present work, we aim to transfer these results to a microplate format. Additionally, we expect that generated metabolic heat can cause an increase in T_s during the proliferation process (Figure 3b). Thus, by simultaneously measuring variations in thermal insulation and temperature, these sensors can enable real-time monitoring of cell proliferation based on cell number, and metabolic activity, respectively.

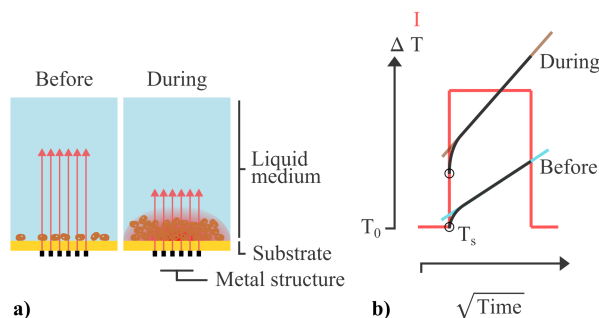


Figure 3: Expected sensor response when measuring cell proliferation. **(a)** During cell proliferation, the number of cells at the sensor interface increases. Simultaneously the cells will generate heat as a result of their metabolism. **(b)** The changing cell number will affect the measured slope, as an increasing number of cells causes an increase in the thermal insulation at the sensor interface. Simultaneously, metabolic heat produced by the cells might result in measurable changes in temperature (T_s).

Methods and materials

Sensor setup

The sensor setup consists of two main parts: A microplate with integrated sensors and a base station with electrical contacts (Figure 4). The in-house designed sensors come in the form of flexible self-adhesive strips (Figure 4a). The fabrication of the sensors was carried out using standard flexible Printed Circuit Board (PCB) manufacturing technology (PCBWay,

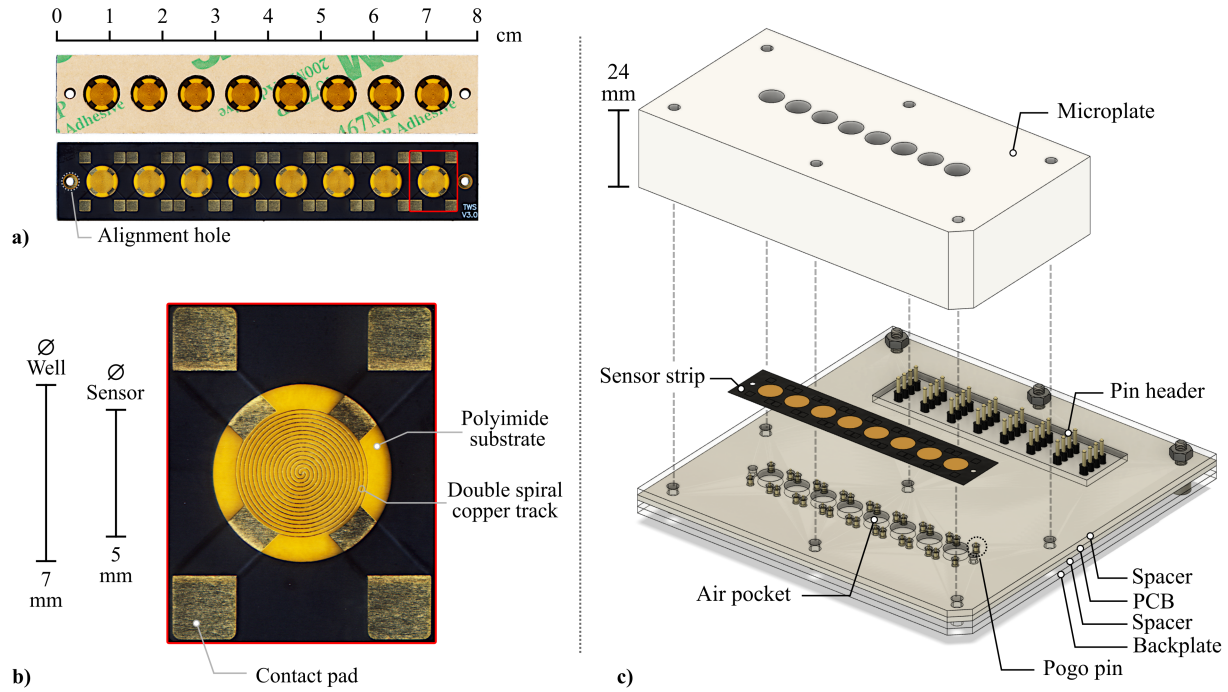


Figure 4: Sensor characteristics and schematic overview of the sensor setup. **(a)** Pictures of both sides of the thin-film sensor strip containing eight individual sensing structures. The top picture shows the release liner of the adhesive side. **(b)** Close-up view of one individual sensor structure. Each double spiral sensing element has four contact pads. **(c)** Exploded view of the total sensor setup with the two main parts: A microplate with sensors incorporated at the bottom and a base station with electrical contacts. The well diameter and spacing of the custom-built microplate are identical to 96-well plate standards.

China). Each strip contains eight individual sensor structures that are specifically designed to fit one 8-well column of a standard 96-well plate.^{49,50} The sensors can be easily integrated into a microplate format by attaching the adhesive side to a bottomless microplate. The adhesive transfer tape (467MP, 3M, United States) (Figure 4a) is sufficient to provide a watertight seal.

Each individual sensor structure exists out of a double spiral copper track that is deposited on a 25 μm thick polyimide substrate (Figure 4b). The copper has an Electroless Nickel Immersion Gold (ENIG) surface finish. The height and width of the copper tracks are 12 μm and 60 μm , respectively. The spacing between the tracks is 80 μm . The spiral sensing element ($\varnothing = 5$ mm) is situated in the center of the well ($\varnothing = 7$ mm) (Figure 4b).

This diameter is conform to 96-well plate standards.^{49,50} Around the sensor structure, four $2\text{ mm} \times 2\text{ mm}$ contact pads are present, which enable a 4-wire resistance measurement of the spiral track. The initial electrical resistance at room temperature (R_{init}) of each structure lies in the range of $3.2\ \Omega$ to $3.6\ \Omega$. The temperature coefficient of electrical resistance was determined experimentally ($\alpha = 3.701 \times 10^{-3} \pm 0.031 \times 10^{-3}\ \text{K}^{-1}$).

As the working principle prescribes, during measurement, Joule heating pulses need to be applied continuously to the sensor structures. In between two heat pulses, it is advised to let the sensor cool back down to ambient temperature to avoid temperature drifts. For this read-out, a standard benchtop Source-Measure Unit (SMU) can be used. We opted for the following default parameters for the sensor read-out in this work: heating power $0.120\ \text{W}$, heating period $1\ \text{s}$, cooling period $120\ \text{s}$, sampling frequency $100\ \text{Hz}$ (during heating step). With these parameters, the ΔT of the sensor during the heating period is approximately 6°C when measuring a well filled with water. The interval in which to perform linear regression was decided to be $[0.0625 - 1]\ \text{s}$, hence $[0.25 - 1]\ \text{s}^{1/2}$. As discussed later, the used parameters can vary slightly depending on the type of experiment.

It should be noted that heating is performed using constant current pulses. As R_{init} varies between sensors, each sensor requires a slightly different heating current to obtain a comparable heating power (P) between sensors. Therefore, before each measurement, R_{init} is measured using a low measurement current of $5\ \text{mA}$. Afterwards, the required heating current (I) for obtaining a specific heating power can be calculated for each sensor using equation (4).^{36,37}

$$I = \sqrt{P/R_{init}} \quad (4)$$

where:

- I = required heating current [A]
- P = desired heating power [W]
- R_{init} = initial electrical resistance [Ω]

The microplate to which the sensor strips are attached (Figure 4c) was designed in-house, and CNC milled out of white Acetal Copolymer (POM-C) (YouniQ Machining, Belgium). POM-C was chosen for its chemical resistance to ethanol, as 70 vol% ethanol is used to clean the wells in between experiments. Alignment holes are present in the bottom of the microplate, as well as in the sensor strips (Figure 4a) to facilitate the correct positioning during fixation using dowel pins. When the sensor strip is attached to the microplate, the sensor structures and contact pads face down. This implies that the metal sensing structure never makes direct contact with the sample inside the well, as the polyimide substrate functions as a thin electrically insulating layer between the structure and the sample, as illustrated in Figure 3. Whilst the diameter and spacing of the wells is equal to the standard 96-well plate format,^{49,50} the depth of the wells is increased to 24 mm (Figure 4c). This increase in depth results in a larger available well volume compared to conventional 96-well plates. Conventional microplates allow for a maximum sample volume of around 300 μ l, whereas the custom microplate enables measurements on samples with volumes up to 600 μ l.

After the sensor strip is attached to the microplate, the microplate is placed on top of the base station for the read-out (Figure 4c). The base station consists of a rigid PCB, which is sandwiched between several polymethyl methacrylate (PMMA) spacer plates. The PCB was designed in-house and fabricated externally (PCBWay, China). The spacer plates were laser cut from 2 mm PMMA slabs (Speedy 100R, Trotec, Austria). For each well, the base station contains four pogo pins (Figure 4c) that make contact with the contact pads present on the sensor strip. Additional cutouts in the top PMMA slab provide a trapped air pocket underneath each individual sensor structure (Figure 4c). This ensures a unidirectional heat transfer as a result of the superior thermally insulating properties of air. To achieve a good

electrical contact, the microplate is fastened to the base station using six bolts and wing nuts (Figure 4c).

Due to its compact size, the sensor setup can be placed inside most standard incubators equipped with a cable access port. For experiments inside an incubator, it is recommended to cover the wells with a lid to reduce evaporation. For this purpose, a custom lid was designed. The lid is slightly elevated (2 mm) by a spacer around the edge that covers all wells. This ensures uniform conditions for all wells under the lid.

Instruments

Two different types of SMU's and multiplexers were used in this work. For the temperature measurement characterization experiments and all experiments on cells, a high-precision PXIe-4139 SMU (NI, USA) was used. This SMU is connected to a PXI-2503 multiplexer switch module (NI, USA), which enables the sequential read-out of up to 12 individual sensor structures. For the characterization experiments on water-ethanol mixtures, a different SMU was used (B2901A, Keysight, USA) in combination with a custom-built 8-channel multiplexer, which allowed faster switching between channels. All SMU's and multiplexers are controlled with a custom LabVIEW program.

For experiments at elevated temperatures, the sensor setup is placed inside an incubator (BD 115, Binder, Germany). Cables from the sensor setup are routed to the SMU outside the incubator via a cable access port. The incubator temperature is read back to the LabVIEW program via two thermocouples (Type K, TC Direct, the Netherlands) and a thermocouple data logger (TC-08, Pico Technology, UK).

To verify the cell number after cell proliferation experiments, a Nanodrop 2000 (Thermo Scientific, USA) is used in cuvette mode.

Temperature measurement characterization

To assess the usability of the sensors as a RTD, characterization experiments were performed. The sensor setup was placed inside an incubator. Initially, the incubator temperature was set to 62 °C and left to stabilize for 8 hours. Afterwards, the temperature was lowered slowly from 62 °C to 22 °C over a period of 15 hours. During the cool down procedure, the electrical resistance of 12 different sensors was measured using two different sensor setups simultaneously. A low measurement current of 5 mA was used to minimize self-heating. To reduce the influence of oven fan noise, styrofoam plugs were inserted into all 12 wells. Two plugs were equipped with miniature thermocouples (Type K, TC Direct, the Netherlands) that touched the bottom of the well, where the metal sensor structure is located. The average temperature of both thermocouples is used as the reference temperature recording. Given the slow-changing temperature profile, and the close contact between the thermocouple and the sensor, we assume that the sensor temperature is equal to the thermocouple temperature at all times.

Characterization of simultaneous temperature- and thermal effusivity measurements

To demonstrate the double function of the sensor to detect variations in temperature as well as thermal effusivity, characterization experiments were performed in which both parameters varied simultaneously. The sensors were read out during the mixing procedure of different water/ethanol volume ratios inside the wells. Upon mixing of water and ethanol in different ratios, the thermal effusivity of the resulting mixture varies accordingly.^{51,52} The thermal effusivity of all different used water/ethanol mixtures was calculated based on values obtained from literature and listed in Table 1. For this, the thermal conductivity (κ) and specific heat (c_p) of pure water and pure ethanol were taken from literature.⁵¹ The κ and c_p values of all water/ethanol mixtures were calculated via the rule of mixtures based on the volume

fraction. The density (ρ) of the water/ethanol mixtures were taken from literature.⁵² Afterwards, e was calculated using equation (3). In addition to the change in e , it is well-known that the mixing of water and ethanol causes an exothermic reaction, which should provoke a measurable transient change in liquid temperature.⁵³

For the experiment, the sensors were read out continuously for a period of 60 minutes. The following parameters were used: heating power 0.120 W, heating period 1 s, cooling period 7 s, sampling frequency 100 Hz. Our suggested default cooling period of 120 s was reduced to 7 s in order to better detect the immediate transient exothermic reaction that occurs upon mixing. Since 8 channels were read out sequentially with a multiplexer, a further reduction in the cooling period was not possible with the used heating period of 1 s.

For the first 30 minutes of the measurements, all wells contained 150 μ l Milli-Q water from Arium pro VF (Sartorius Stedim Biotech, Germany). After 30 minutes, 150 μ l of different water/ethanol mixtures (0, 20, 40, 60, 80, and 100 vol% ethanol) were added and resuspended. Resuspension ensured a good mixing of the fluids, resulting in a homogeneous mixture. The resulting volume percentages of ethanol at the end of the experiment were 0, 10, 20, 30, 40, and 50 vol%. Each dilution was measured five times with different individual sensor structures. This results in a total of 30 mixing experiments.

All used ethanol dilutions were prepared in advance using Ethanol absolute $\geq 99.8\%$ (VWR, Belgium). Afterwards, all liquids were stored at room temperature to ensure that they were at identical temperature at the time of the experiments.

Table 1: Material properties of used liquids^{51,52}

	κ	ρ	c_p	e
	[W/mK]	[kg/m ³]	[J/kgK]	[Ws ^{1/2} /m ² K]
Ethanol	0.180	791	2440	589
50 vol%	0.392	932	3312	1099
40 vol%	0.434	950	3486	1198
30 vol%	0.476	964	3661	1296
20 vol%	0.518	975	3835	1392
10 vol%	0.561	987	4010	1489
Water	0.603	1000	4184	1588

Relative quantification of the number of cells at the interface in the absence of growth

To verify whether the sensors are able to distinguish between varying numbers of cells at the sensor interface based on the measured thermal insulation, we have conducted cell sedimentation experiments. By letting cell suspensions of different concentrations sediment inside the wells, it is possible to vary the number of cells at the sensor surface in a controlled manner. For these experiments, our default measurement parameters were used: heating power 0.120 W, heating period 1 s, cooling period 120 s, sampling frequency 100 Hz.

Cell suspensions were made of freeze-dried *Saccharomyces cerevisiae* (Dr. Oetker, Germany) in Milli-Q water (0, 1, 2, 4, 8, 10, 14, 18, 22, and 26 mg/ml) without the addition of nutrients. These suspensions were made within one hour before the experiment. No efforts were made to determine the actual cell count. However, as dilutions were made from the suspension with the highest concentration, it can be assumed that the number of cells varies in accordance with the concentration. All suspensions were thoroughly resuspended, and 300 μ l of each suspension was pipetted into different wells. The data recording was started immediately after addition and left to run for 12 hours.

Cell proliferation experiment with varying nutrient contents

The intention of this experiment is to demonstrate that the presented sensor device can be used to monitor cell proliferation by a simultaneous relative quantification of cell number and metabolic activity. This is done by measuring increments in thermal insulation at the interface caused by an increasing number of cells and by simultaneously monitoring changes in temperature caused by the generated metabolic heat of differently sized cell populations. For validation purposes, growth media with three different nutrient contents were used for the proliferation experiments. It is expected that the wells with the highest nutrient content will contain the largest final cell number at the end of the experiment, as well as the highest metabolic heat generation during the proliferation process. To verify the cell number before and after the experiments, the optical density of the cell cultures is read at 600 nm (OD_{600}) using a Nanodrop 2000 (Thermo Scientific, USA) in cuvette mode. All OD_{600} measurements are performed after making a 1/10 dilution using fresh medium with the appropriate nutrient content.

Throughout this experiment, a total number of 12 wells was measured using the standard measurement parameters. Before starting the experiment, the microplate wells were cleaned with 70 vol% ethanol and blow-dried with nitrogen. The proliferation experiments were performed inside an incubator at 30 °C. Therefore, the sensor setup was placed inside the incubator for four hours in advance to allow the microplate to reach a stable temperature before the experiments.

Freeze-dried yeast (*Saccharomyces cerevisiae*) was chosen as a test organism, identical to the type used in the cell sedimentation experiments described in the previous section. Yeast Peptone Dextrose (YPD) medium was used as the nutrient source (VWR, Belgium). This YPD broth is supplied as a pre-mixed powder that can be dissolved in water. The nutrient content was varied by using different YPD concentrations. We label the manufacturers' recommended YPD concentration of 50 g/l as 100% nutrient content. The used nutrient contents in the experiments are 100%, 50%, and 25%. All different concentrations were

measured in triplicate by filling three wells with each of the three different media. The remaining three wells were filled with MilliQ water as a reference. The temperatures measured in the reference wells are used to subtract the incubator temperature fluctuations from the temperature measurements of all other wells. This approach of using wells filled with water to subtract ambient temperature fluctuations was taken from a study by Wasdö et al. in which a novel type of isothermal microcalorimeter was presented.²¹

Shortly before the start of the data recording, the wells were filled with 600 μl of the different growth media and Milli-Q water. At this stage, no cells are added yet. After allowing the liquids to reach a stable temperature for three hours, 8 μl of *Saccharomyces cerevisiae* stock solution ($\text{OD}_{600} = 1.07$) was added to each well containing YPD medium. The stock solution was prepared 24 hours before the experiment and was thoroughly resuspended before usage. The data recording continued for a total period of approximately 44 hours. Directly after the experiment, the OD_{600} of all cell cultures inside the wells was measured to obtain a relative quantification of the final cell number after proliferation.

Results and Discussion

Temperature measurement characterization

Figure 5 shows the measured resistance of 12 sensors at incubator temperatures between 22 °C and 62 °C. The results confirm the expected linear relationship between the temperature and electrical resistance. From these data, the temperature coefficient of the electrical resistance (α) was determined between 25 °C and 35 °C ($\alpha = 3.701 \times 10^{-3} \pm 0.031 \times 10^{-3} \text{ K}^{-1}$). This value complies with α values of copper that can be found in literature.⁵⁴ Furthermore, Figure 5 shows that the initial electrical resistance (R_{init}) of the sensors varies between 3.2 Ω and 3.6 Ω . This is due to variations in the manufacturing process of the metal structures. The results confirm that the sensors can be used for absolute temperature measurements at the bottom of the microplate wells.

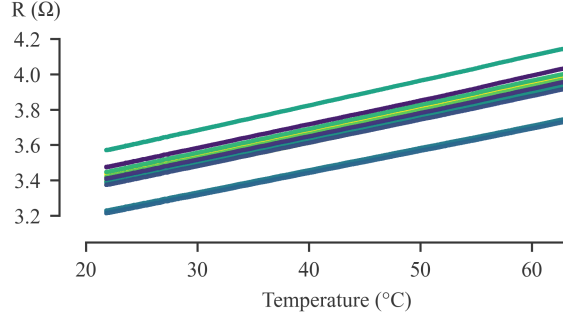


Figure 5: The electrical resistance of 12 randomly selected sensors was monitored over a wide temperature range (22 °C to 62 °C). The results confirm that the sensors are suited for monitoring the temperature at the bottom of microplate wells.

Characterization of simultaneous temperature- and thermal effusivity measurements

To assess whether the sensors can simultaneously detect variations in temperature and thermal effusivity, different volume ratios of water and ethanol were mixed inside the wells. Meanwhile, pulses were applied continuously. To give one example, Figure 6 shows all sensor temperature response curves measured during one experiment on the mixing of 150 μl of water with 150 μl of pure ethanol, resulting in a final mixture of 50 vol% ethanol. For the first 30 minutes of the experiment, only water was present inside the well. The rise

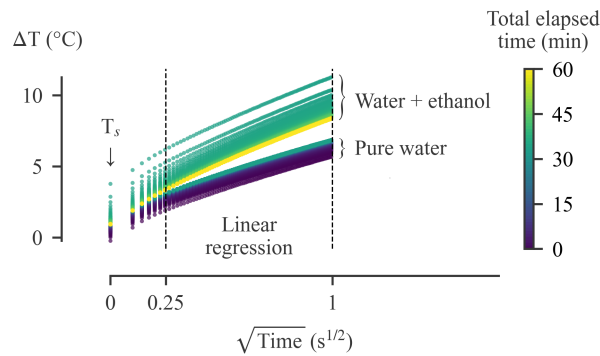


Figure 6: Characterization experiments were performed on the simultaneous measurement of temperature and thermal effusivity (e) by monitoring the mixing of different water/ethanol volume ratios inside a well. This plot shows all temperature response curves of one sensor structure, taken continuously for 60 minutes, during the mixing of pure water and ethanol. Immediately after the addition of ethanol to water at minute 30, an increase in both T_s and slope is observed.

in the first temperature recording at the start of a pulse (T_s) during the first 15 minutes indicates that there is a drift in liquid temperature (Figure 6). This can be explained by the short cooling period of 7 s, which is not sufficient for the liquid to cool down to ambient temperature in between heat pulses. Despite this drift in T_s , all slopes measured in water are equal, as all sensor temperature response curves are practically parallel (Figure 6). At minute 30, pure ethanol is added to the water and resuspended. Immediately, an increase in T_s occurs (Figure 6). This can be explained by the rise in liquid temperature caused by the exothermic reaction of water and ethanol. Furthermore, as expected, the slope increases due to the lower thermal effusivity of the final water/ethanol mixture compared to pure water (Table 1). For all subsequent sensor response curves, T_s decreases, whilst the curves remain parallel to the first curve measured on the mixture. This result (Figure 6) confirms the hypothesis that changes in thermal effusivity (Figure 1) and changes in temperature (Figure 2) can be measured simultaneously.

To evaluate the sensor sensitivity and inter-sensor reproducibility, the water/ethanol mixing procedure was repeated with six different water/ethanol ratios. Five replicates were measured for each mixing ratio. The measured changes in slope and T_s are discussed below.

To analyze the slopes of the temperature curves in detail, we performed linear regressions on all curves within the time interval of $[0.25 - 1] \text{ s}^{1/2}$, as indicated in Figure 6. The obtained slopes are plotted as a function of time in Figure 7a. More specifically, this plot shows the percentage change in slope relative to the slope measured in water. This procedure of plotting the percentage change in slope eliminates the influence of the difference in R_{init} between sensors.^{36,37} Figure 7a highlights that the sensors show a fast and reproducible response to changes in the thermal effusivity of the sample. In this experiment, the limiting factor for the sensor response time is the required cooling time of 7 s between the heating steps.

Figure 7b shows all measured changes in slope between the minutes 40 en 45 as a function of the final volume percent of the water/ethanol mixture. This graph shows that the

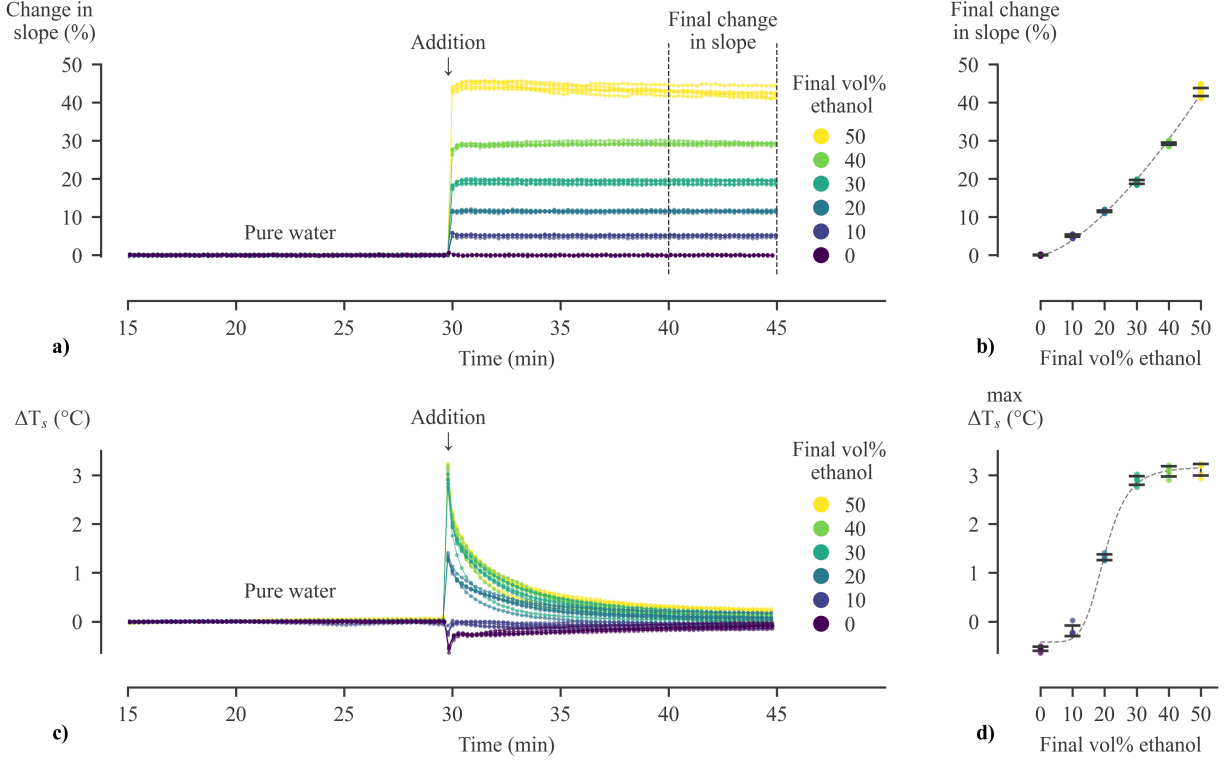


Figure 7: To demonstrate the ability of the sensors to simultaneously measure temperature and thermal effusivity (e), the experiment presented in Figure 6 was repeated with six different water/ethanol mixtures. Five replicates were measured for each mixing ratio. **(a)** All final water/ethanol mixtures have a distinct e , as listed in Table 1. The difference in e can be derived from the measured slopes. This time-series plot highlights the fast response of the sensors to changes in e of the sample inside the well. **(b)** The final change in slope of all measurements plotted as a function of the final ethanol volume fraction. **(c)** ΔT_s of all experiments plotted as a function of time. This plot indicates that the sensors also show a fast response to changes in the temperature of the sample inside the well. **(d)** The maximum temperature difference of all measurements plotted as a function of the final ethanol volume fraction.

measured slope can be used to distinguish between all different water/ethanol mixtures. Furthermore, this graph displays the good inter-sensor reproducibility.

Figure 7c shows ΔT_s of all 30 experiments over time measured between minutes 15 and 45. At the start of this period, the water sample has reached a stable temperature after the initial heat-up. At the end of this period, the sample temperature is stabilized again after the addition step. In this plot, the stable temperatures between minutes 15 and 20 are chosen as a baseline (0 °C). It can be clearly seen that mixing water and ethanol causes an

immediate rise in T_s , whilst adding 150 μl of pure water at room temperature has a cooling effect on the heated water that is already present inside the well (Figure 7c). This graph highlights that the sensors also show a fast response to changes in liquid temperature.

Figure 7d shows the relation between the maximum change in T_s , and the final concentration of the water/ethanol mixture. It should be noted that the standard deviation on this maximum measured temperature change is also influenced by the possible time difference of maximum 7 s between the moment of addition and the measurement.

To quantify the precision and accuracy of the sensors for measuring e , a calibration curve is constructed to convert the measured changes in slope to actual values of e expressed in $\text{Ws}^{1/2}/\text{m}^2\text{K}$. To obtain this calibration curve, first, the final slope values plotted in Figure 7b are plotted versus the actual e of the final water/ethanol mixtures (Figure 8a). For this, the actual e values obtained from literature are used (Table 1). A quadratic regression ($y = ax^2 + bx + c$) is performed ($R^2 = 0.99$) where: $a = 1.069 \times 10^{-4}$, $b = -3.739 \times 10^{-1}$ and $c = 324.3$, see Figure 8a. This quadratic equation can be used to convert the measured change in slope to a measured value of e (Figure 8b). On average, the sensors measure e accurately within 0.39%, with a precision of $4.5 \text{ Ws}^{1/2}/\text{m}^2\text{K}$ within the explored range. The exact accuracy and precision of these experiments are given in Table 2.

These measurements on the mixing of water and ethanol demonstrate the potential of the methodology. The experiments show that the setup can simultaneously detect changes in e , as well as changes in temperature. Notably, these results highlight the fast responsiveness of the sensor to both measurands as well as the high inter-sensor reproducibility.

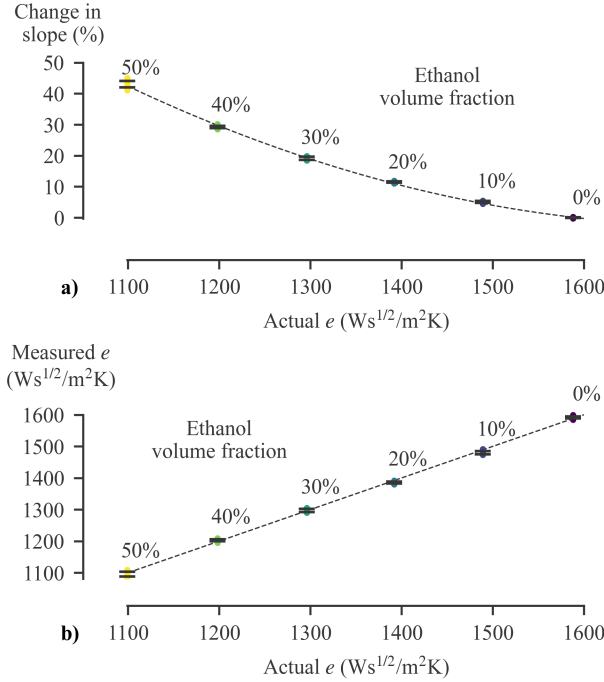


Figure 8: Calibration of the sensors for measuring absolute thermal effusivity. **(a)** Final change in slope in function of the actual e as taken from literature (Table 1). The relation between the measured change in slope and the actual e can be approximated by a quadratic regression, which can be used as a calibration curve. **(b)** The measured slope changes can be converted to absolute values of thermal effusivity using the obtained calibration equation. The resulting measured e values are plotted as a function of the actual e derived from literature. Within the studied range, the sensors can determine e with an average accuracy of 0.39% and a precision of $4.5 \text{ Ws}^{1/2}/\text{m}^2\text{K}$

Table 2: Accuracy and precision of measurements of thermal effusivity (e)

Actual e [$\text{Ws}^{1/2}/\text{m}^2\text{K}$]	Mean Measured e [$\text{Ws}^{1/2}/\text{m}^2\text{K}$]	Accuracy [%]	Standard Deviation [$\text{Ws}^{1/2}/\text{m}^2\text{K}$]
1099	1096.0	0.27	7.6
1198	1203.9	0.49	3.1
1296	1298.0	0.15	5.1
1392	1386.7	0.38	2.8
1489	1482.7	0.42	5.1
1588	1597.5	0.60	3.2
Average		0.39	4.5

Relative quantification of the number of cells at the interface in the absence of growth

Thermal pulses were applied continuously during the sedimentation of cell suspensions with different concentrations. Figure 9a shows the percentage change in slope of all pulses over time, relative to the slope of the first applied pulse. It is assumed that all cells are still in suspension at the time of the first pulse. Afterwards, cells are expected to accumulate at the sensor surface. Within the first 2 hours of sedimentation, the plot shows considerable changes in slope, especially for experiments with higher cell concentrations. In this time period, the slopes increase because of the thermal insulation effect of the cells that accumulate at the sensor-liquid interface. After approximately 2 hours, the slopes do no longer change (Figure 9a). From this, we conclude that, at this time, the sedimentation process is completed for all cell concentrations. After sedimentation, it is clear that different numbers of cells cause different measurable changes in thermal insulation at the sensor interface.

In Figure 9b, all data points taken after sedimentation, i.e. after hour 2 (Figure 9a), are plotted against the concentration of the used cell suspension. This plot indicates that the relationship between the cell concentration and the final change in slope is linear before saturation occurs at a maximum change in slope of approximately 8%. More specifically, the maximum measured change in slope of the linear sensing range is 6.43%. This limit is indicated by a horizontal dashed line in Figure 9b. Our earlier study on thermal-based thin film thickness determination showed that saturation occurs when the thickness of the film at the sensor interface exceeds the probing depth of the applied thermal pulses.³⁶ Furthermore, this previous study showed that the measured change in slope is dependant on the difference in the thermal effusivity between the film and the medium above.³⁶ Thus, in the current experiment, the maximum measurable change in slope of 8% is also dependant on the difference in the thermal effusivity between the used cells and water. Below the saturation level, the linear sensor response indicates that the measured change in slope can be used as a direct measure of relative changes in the number of cells at the interface. These results

are consistent with our earlier findings.³⁷ Furthermore, these results suggest that the presented sensors can be used for the real-time monitoring of cell number during proliferation experiments.

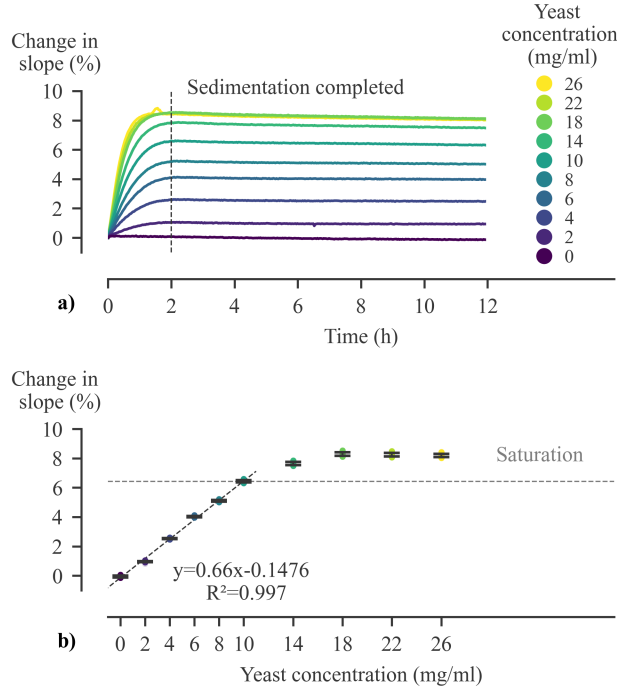


Figure 9: Measuring the thermal insulation effect of cells at the sensor interface. **(a)** The number of cells at the sensor interface was varied by letting cell suspensions of different concentrations sediment inside the wells (*Saccharomyces cerevisiae* in water). The change in slope was registered continuously during the sedimentation process. The time series plot shows that the sedimentation is completed after approximately 2 hours, regardless of the cell concentration. **(b)** When plotting the final change in slope (all measured slopes after 2 hours) as a function of the concentration of the used yeast suspension, it is possible to observe a linear relationship before saturation occurs. This linear relationship indicates that, below the saturation level, the measured change in slope can be used as a direct measure of relative changes in the number of cells at the interface.

Cell proliferation experiment with varying nutrient contents

Proliferation experiments are performed in growth media with three different nutrient contents. It is expected that the wells with the highest nutrient content will contain the highest cell number at the end of the experiment, and consequently, the highest metabolic heat generation during the experiment. The purpose of these experiments is to evaluate whether

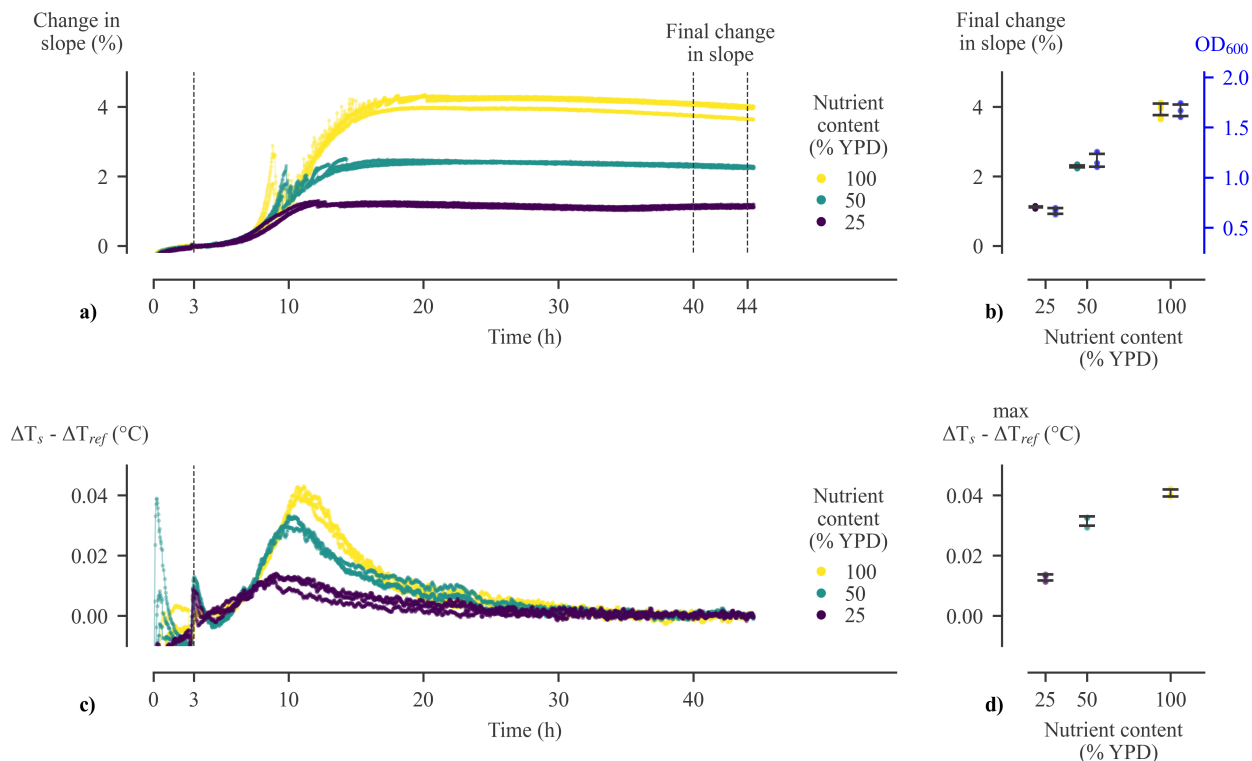


Figure 10: Monitoring cell proliferation by relative quantification of cell number and metabolic activity. The growth of *Saccharomyces cerevisiae* was studied in triplicate for media with different nutrient contents (25, 50, and 100% YPD). The three remaining wells were filled with water as a reference. **(a)** To investigate variations in cell number, the percentage change in slope is plotted as a function of time. The results indicate that, with higher nutrient contents, the proliferation is sustained for a longer period of time. Consequently, the final cell number is higher for media with higher nutrient content. **(b)** The final measured change in slope shows good agreement with the OD₆₀₀ measured at the end of the proliferation experiment. **(c)** After processing the ΔT_s data, three distinct temperature profiles can be observed based on the nutrient content of the growth media. This indicates that the sensors are sufficiently accurate to detect the metabolic activity of biological cells in a microplate format. **(d)** The maximum temperature difference measured during growth as a function of the nutrient content. This plot indicates that more metabolic heat is being generated when more actively growing cells are present on the sensor surface.

both signals can be derived from the measured sensor temperature response curves.

First, we address the monitoring of variations in cell number. Therefore, the slopes of the sensor response curves are analyzed. Figure 10a shows the percentage change in slope over time, relative to the slope measured at hour 3, immediately after the addition of cells to the wells containing growth media. At this time, an equal number of cells is present in all

nine wells. Figure 10a shows that, after an initial lag phase, the slopes start to rise for all measurements, indicating that cells are multiplying at the interface. Three distinct growth curves can be observed based on the nutrient content. From the growth curves, it is clear that, as more nutrients are available, proliferation can be sustained for a longer period. This results in a higher final number of cells at the interface, and thus a larger final slope at the end of the proliferation process (Figure 10a).

Around the 10 hour mark, temporary fluctuations in slope are visible, most notably on the measurements with 100% and 50% nutrient content (Figure 10a). We assign these fluctuations to the formation of gas bubbles during the proliferation process. As gas bubbles form on the sensor surface, the thermal insulation increases. This can result in sudden increases in slope. However, as these gas bubbles detach or dissolve, the slopes can drop equally fast.

The slope measurements are summarized in Figure 10b. This plot shows the final change in slope (between hours 40 and 44, see Figure 10a) as a function of the nutrient content. Additionally, this plot contains the OD_{600} value of all cell suspensions measured at the end of the experiment. This plot indicates good agreement between the final change in slope, and the final OD_{600} value. The conformity between the thermal and optical measurements can be explained by the fact that both sensors are working inside their linear range. The maximum measured change in slope of approximately 4%, measured for media with the highest nutrient content (Figure 10b), is well below the previously demonstrated limit of the linear sensor range of 6.43% (Figure 9b). The linear response of the optical readout is ensured by making 1/10 dilutions before measuring the OD_{600} value.

Secondly, we address the sensing of the metabolic activity. The intention was to detect heat generated by the metabolic activity from changes in T_s . In previous characterization experiments, performed at room temperature, raw values of ΔT_s were discussed (Figure 7c). However, with these proliferation experiments, performed inside an incubator at 30 °C, raw values of ΔT_s did not render clear results. The raw ΔT_s signal contained fluctuations coming

from the incubator temperature control, as well as a small temperature drift, presumably caused by the slow heating up of the microplate itself. Therefore, the average temperature measured in the three reference wells (ΔT_{ref}) was subtracted from the ΔT_s of the nine wells containing cell cultures. Afterwards, the data was linearly detrended. The resulting data is plotted in Figure 10c. In this plot, after hour 3, distinct temperature profiles can be observed based on the nutrient content of the growth media. As expected, measurements on media with high nutrient content showed a higher increase in T_s . Before and shortly after the first three hours, the plot shows random fluctuations in temperature, even after the data processing. These fluctuations are mainly caused by the disturbance of the incubator temperature that occur because of the opening and closing of the door, which is required to add the growth media and cells to the wells. To summarize the results, the maximum temperature of a 10-point moving average of these data is plotted as a function of the nutrient content in Figure 10d. The results confirm that metabolic activity can be measured.

It is important to bear in mind that in these proliferation experiments (Figure 10), media with different nutrient contents were used whilst the saturation level of the sensor was determined through cell sedimentation experiments performed in water containing no nutrients at all. Previously, in the discussion of the sedimentation experiments, we pointed out that differences in thermal effusivity of the media might affect the measured change in slope, and thus may lead to errors in the data interpretation. However, because of the relatively low nutrient contents (5, 2.5, and 1.25 wt% in water) we assume this influence is minimal. The good agreement between the measured changes in slope and the OD_{600} measurements further support this conclusion. Additionally, to avoid any possible influence of differences in the composition of the medium, we have repeated the experiments as presented in Figure 10, in wells containing an identical medium (100% YPD), but with a varying starting cell concentration. These results, presented in the Supporting Information, are consistent with those of Wasdö et al.¹⁵ who found that a decreasing starting cell concentration results in a longer lag phase and lower peaks in the metabolic activity curves. This agreement with literature

confirms the correct working of the presented sensors.

In conclusion, the results point out the potential use of this thermal sensing technique for monitoring cell proliferation. The sensors enable the simultaneous real-time detection of changes in metabolic activity and cell number. Variations in cell number are visible directly from the measured slope of the temperature response curves. For visualizing the metabolic activity, additional data processing is required to remove the environment temperature noise from the signal.

The hardware used for these proof-of-principle experiments was limited to 12 channels. However, we foresee no insurmountable issues in scaling up this technology to a standard 96-well plate format. With the presented experiments, a heating period of 1 s was used in combination with a cooling period of 120 s. This implies that it is possible to read out up to 120 wells with a single SMU, provided that a larger multiplexer is available.

Conclusion

In this work, we have developed novel thin-film thermal sensors specifically designed to fit inside the well diameter of standard 96-well plates. The design is inspired by the Transient Plane Source (TPS) sensor design (also called Hot Disk sensor). The fabrication of the sensors was done using standard flex PCB manufacturing technology. The intention was to demonstrate the usability of these sensors as a real-time and label-free microplate reader technology based on measurements of temperature and thermal properties. For the read-out of the sensors, only a single benchtop 4-wire Source-Measure Unit (SMU) is required, preferably in combination with a multiplexer to allow for the parallel read-out of multiple wells.

Initially, the sensor's ability to simultaneously measure temperature as well as thermal effusivity was demonstrated by characterization experiments on water/ethanol mixtures. These experiments highlighted the fast response of the sensor to changes in temperature as

well as thermal effusivity. In principle, even faster sensor response times can be achieved, as currently, the required cool time between measurements is the main limiting factor of the sensor response time. Additionally, these characterization experiments showed the excellent reproducibility between sensors. A general calibration curve was constructed to convert the measured sensor temperature responses to absolute values of thermal effusivity. Currently, for this calibration, one reference measurement in water is required for each sensor. Afterwards, within the explored range of 1100 to 1600 $\text{Ws}^{1/2}/\text{m}^2\text{K}$, the thermal effusivity of samples inside the wells can be determined with an accuracy of 0.39%, and a standard deviation of 4.5 $\text{Ws}^{1/2}/\text{m}^2\text{K}$. It should be noted, however, that the achievable accuracy and precision strongly depends on the specifications of the used SMU.

To demonstrate the usability of this thermal-based microplate reader for monitoring cell proliferation, proof-of-principle experiments were performed on *Saccharomyces cerevisiae* in liquid media with different nutrient contents. All presented proliferation experiments were performed inside a standard incubator at elevated temperature. We demonstrated that it was possible to derive changes in cell number from the sensor temperature response curves. Moreover, it was shown that the slope of the measured curves increase linearly with the number of cells at the sensor surface. Simultaneously, it was possible to measure differences in the metabolic heat generated by the differently sized cell populations. Additional proliferation experiments presented in the Supporting Information further confirmed these findings.

The current study was limited to experiments on *Saccharomyces cerevisiae*, however, the results indicate that the presented technique might also be used for monitoring bacterial growth based on quantity and metabolic activity. In case the difference in thermal effusivity between the test organism and the medium is sufficiently large, it might also be possible to monitor changes in the partial cell coverage of a monolayer whilst simultaneously monitoring the metabolic activity of the monolayer. Demonstrating these possible applications through future research could further expand the usefulness of the proposed technique.

In summary, the presented sensors have proven to be capable of monitoring cell proliferation based on simultaneous relative measurements of cell number and metabolic activity. Moreover, the measurement principle is real-time, and requires no auxiliary chemicals that might influence the intrinsic cell behavior. This makes the technology especially suited for the study of biological questions with unknown timing and duration. The current study was limited to a 12-channel read-out device. However, the findings suggest that the technology can be scaled up to a 96-channel device for the read-out of standard 96-well plates. This way, the technology can also be used for parallelized drug screening and toxicity assays.

Associated Content

Supporting Information

Additional experiment: monitoring cell proliferation using identical media with varying start cell concentration (PDF)

Acknowledgment

The authors kindly acknowledge support for this work by the Research Foundation Flanders FWO within the project G.0791.16.N. Furthermore, this work is funded by the BIOMAT project, which is carried out under Interreg VA Grensregio Vlaanderen – Nederland and is supported by the European Union and The European Regional Development Fund and with the financial support of the Province of Limburg – Belgium. We thank Daniel Nieder for the initial preliminary experiments and Senne Seneca for stimulating discussions. Thanks to Makerspace PXL/UHasselt for the technical support.

References

- (1) Adan, A.; Kiraz, Y.; Baran, Y. Cell Proliferation and Cytotoxicity Assays. *Current Pharmaceutical Biotechnology* **2016**, *17*, 1213–1221.
- (2) Jones, E.; Michael, S.; Sittampalam, G. S. Basics of Assay Equipment and Instrumentation for High Throughput Screening. *Assay Guidance Manual [Internet]* **2016**,
- (3) Hamalainen-Laanaya, H.; Orloff, M. Analysis of Cell Viability using Time-Dependent Increase in Fluorescence Intensity. *Analytical Biochemistry* **2012**, *429*, 32–38.
- (4) Ou, F.; McGoverin, C.; Swift, S.; Vanholsbeeck, F. Rapid and Cost-Effective Evaluation of Bacterial Viability using Fluorescence Spectroscopy. *Analytical and Bioanalytical Chemistry* **2019**, *411*, 3653–3663.
- (5) Sali, N.; Nagy, S.; Poór, M.; Kőszegi, T. Multiparametric Luminescent Cell Viability Assay in Toxicology Models: A Critical Evaluation. *Journal of Pharmacological and Toxicological Methods* **2016**, *79*, 45–54.
- (6) Tominaga, H.; Ishiyama, M.; Ohseto, F.; Sasamoto, K.; Hamamoto, T.; Suzuki, K.; Watanabe, M. A Water-Soluble Tetrazolium Salt Useful for Colorimetric Cell Viability Assay. *Analytical Communications* **1999**, *36*, 47–50.
- (7) Single, A.; Beetham, H.; Telford, B. J.; Guilford, P.; Chen, A. A Comparison of Real-Time and Endpoint Cell Viability Assays for Improved Synthetic Lethal Drug Validation. *Journal of Biomolecular Screening* **2015**, *20*, 1286–1293.
- (8) Duellman, S. J.; Zhou, W.; Meisenheimer, P.; Vidugiris, G.; Cali, J. J.; Gautam, P.; Wennerberg, K.; Vidugiriene, J. Bioluminescent, Nonlytic, Real-Time Cell Viability Assay and use in Inhibitor Screening. *Assay and Drug Development Technologies* **2015**, *13*, 456–465.

- (9) Lehtinen, J.; Järvinen, S.; Virta, M.; Lilius, E.-M. Real-Time Monitoring of Antimicrobial Activity with the Multiparameter Microplate Assay. *Journal of Microbiological Methods* **2006**, *66*, 381–389.
- (10) Ke, N.; Wang, X.; Xu, X.; Abassi, Y. A. *Mammalian Cell Viability*; Springer, 2011; pp 33–43.
- (11) Chiu, C.-H.; Lei, K. F.; Yeh, W.-L.; Chen, P.; Chan, Y.-S.; Hsu, K.-Y.; Chen, A. C.-Y. Comparison Between xCELLigence Biosensor Technology and Conventional Cell Culture System for Real-Time Monitoring Human Tenocytes Proliferation and Drugs Cytotoxicity Screening. *Journal of Orthopaedic Surgery and Research* **2017**, *12*, 1–13.
- (12) Chawla, K.; Modena, M. M.; Ravaynia, P. S.; Lombardo, F. C.; Leonhardt, M.; Panic, G.; Burgel, S. C.; Keiser, J.; Hierlemann, A. Impedance-Based Microfluidic Assay for Automated Antischistosomal Drug Screening. *ACS Sensors* **2018**, *3*, 2613–2620.
- (13) Nikotina, A. D.; Koludarova, L.; Komarova, E. Y.; Mikhaylova, E. R.; Aksenov, N. D.; Suezov, R.; Kartzev, V. G.; Margulis, B. A.; Guzhova, I. V. Discovery and Optimization of Cardenolides Inhibiting HSF1 Activation in Human Colon HCT-116 Cancer Cells. *Oncotarget* **2018**, *9*, 27268.
- (14) Sijben, H. J.; van den Berg, J. J.; Broekhuis, J. D.; IJzerman, A. P.; Heitman, L. H. A Study of the Dopamine Transporter using the TRACT Assay, a Novel in vitro Tool for Solute Carrier Drug Discovery. *Scientific Reports* **2021**, *11*, 1–14.
- (15) Wadsö, I. Isothermal Microcalorimetry in Applied Biology. *Thermochimica Acta* **2002**, *394*, 305–311.
- (16) Ma, J.; Qi, W.; Yang, L.; Yu, W.; Xie, Y.; Wang, W.; Ma, X.; Xu, F.; Sun, L. Microcalorimetric Study on the Growth and Metabolism of Microencapsulated Microbial Cell Culture. *Journal of Microbiological Methods* **2007**, *68*, 172–177.

- (17) Braissant, O.; Theron, G.; Friedrich, S. O.; Diacon, A. H.; Bonkat, G. Comparison of Isothermal Microcalorimetry and BACTEC MGIT960 for the Detection of the Metabolic Activity of Mycobacterium Tuberculosis in Sputum Samples. *Journal of Applied Microbiology* **2020**, *128*, 1497–1502.
- (18) Butini, M. E.; Moreno, M. G.; Czuban, M.; Koliszak, A.; Tkhilaishvili, T.; Trampuz, A.; Di Luca, M. *Advances in Microbiology, Infectious Diseases and Public Health*; Springer, 2018; pp 61–77.
- (19) Lerchner, J.; David, K.; Unger, F.; Lemke, K.; Förster, T.; Mertens, F. Continuous Monitoring of Drug Effects on Complex Biological Samples by Segmented Flow Chip Calorimetry. *Journal of Thermal Analysis and Calorimetry* **2017**, *127*, 1307–1317.
- (20) Braissant, O.; Keiser, J.; Meister, I.; Bachmann, A.; Wirz, D.; Göpfert, B.; Bonkat, G.; Wadsö, I. Isothermal Microcalorimetry Accurately Detects Bacteria, Tumorous Microtissues, and Parasitic Worms in a Label-Free Well-Plate Assay. *Biotechnology Journal* **2015**, *10*, 460–468.
- (21) Wadsö, I.; Hallén, D.; Jansson, M.; Suurkuusk, J.; Wenzler, T.; Braissant, O. A Well-Plate Format Isothermal Multi-Channel Microcalorimeter for Monitoring the Activity of Living Cells and Tissues. *Thermochimica Acta* **2017**, *652*, 141–149.
- (22) Gustafsson, S. E.; Karawacki, E.; Khan, M. N. Transient Hot-Strip Method for Simultaneously Measuring Thermal Conductivity and Thermal Diffusivity of Solids and Fluids. *Journal of Physics D: Applied Physics* **1979**, *12*, 1411.
- (23) Gustavsson, M.; Karawacki, E.; Gustafsson, S. E. Thermal Conductivity, Thermal Diffusivity, and Specific Heat of Thin Samples from Transient Measurements with Hot Disk Sensors. *Review of Scientific Instruments* **1994**, *65*, 3856–3859.
- (24) Gustafsson, S. E. Transient Plane Source Techniques for Thermal Conductivity and

Thermal Diffusivity Measurements of Solid Materials. *Review of Scientific Instruments* **1991**, *62*, 797–804.

- (25) International Organization for Standardization (ISO). (2015) ISO 22007-2:2015(en) Plastics — Determination of Thermal Conductivity and Thermal Diffusivity — Part 2: Transient Plane Heat Source (Hot Disc) Method. [Online]. Available: <https://www.iso.org/obp/ui/#iso:std:iso:22007:-2:ed-2:v1:en>, retrieved on 2020/05/06.
- (26) Dixon, C.; Strong, M. R.; Zhang, S. M. Transient Plane Source Technique for Measuring Thermal Properties of Silicone Materials used in Electronic Assemblies. Proceedings of SPIE - The International Society For Optical Engineering. 2000; pp 362–370.
- (27) Berge, A.; Adl-Zarrabi, B.; Hagentoft, C.-E. Determination of Specific Heat Capacity by Transient Plane Source. *Frontiers of Architectural Research* **2013**, *2*, 476–482.
- (28) Benazzouk, A.; Douzane, O.; Mezreb, K.; Laidoudi, B.; Quéneudec, M. Thermal Conductivity of Cement Composites Containing Rubber Waste Particles: Experimental Study and Modelling. *Construction and Building Materials* **2008**, *22*, 573–579.
- (29) Malinarič, S. Contribution to the Transient Plane Source Method for Measuring Thermophysical Properties of Solids. *International Journal of Thermophysics* **2013**, *34*, 1953–1961.
- (30) Johansson, P.; Adl-Zarrabi, B.; Hagentoft, C.-E. Using Transient Plane Source Sensor for Determination of Thermal Properties of Vacuum Insulation Panels. *Frontiers of Architectural Research* **2012**, *1*, 334–340.
- (31) Harris, A.; Kazachenko, S.; Bateman, R.; Nickerson, J.; Emanuel, M. Measuring the Thermal Conductivity of Heat Transfer Fluids via the Modified Transient Plane Source (MTPS). *Journal of Thermal Analysis and Calorimetry* **2014**, *116*, 1309–1314.

- (32) Liu, B.; Wang, H.; Qin, Q.-H. Modelling and Characterization of Effective Thermal Conductivity of Single Hollow Glass Microsphere and its Powder. *Materials* **133**, **2018**, *11*.
- (33) Ahadi, M.; Andisheh-Tadbir, M.; Tam, M.; Bahrami, M. An Improved Transient Plane Source Method for Measuring Thermal Conductivity of Thin Films: Deconvoluting Thermal Contact Resistance. *International Journal of Heat and Mass Transfer* **2016**, *96*, 371–380.
- (34) Zhang, H.; Li, M.-J.; Fang, W.-Z.; Dan, D.; Li, Z.-Y.; Tao, W.-Q. A numerical Study on the Theoretical Accuracy of Film Thermal Conductivity using Transient Plane Source Method. *Applied Thermal Engineering* **2014**, *72*, 62–69.
- (35) Kyoo Park, B.; Yi, N.; Park, J.; Kim, D. Thermal Conductivity of Single Biological Cells and Relation with Cell Viability. *Applied Physics Letters* **2013**, *102*, 203702.
- (36) Oudebrouckx, G.; Vandenryt, T.; Nivelles, P.; Bormans, S.; Wagner, P.; Thoelen, R. Introducing a Thermal-Based Method for Measuring Dynamic Thin Film Thickness in Real Time as a Tool for Sensing Applications. *IEEE Transactions on Instrumentation and Measurement* **2020**, *70*, 1–10.
- (37) Bormans, S.; Oudebrouckx, G.; Vandormael, P.; Vandenryt, T.; Wagner, P.; Somers, V.; Thoelen, R. Pulsed Thermal Method for Monitoring Cell Proliferation in Real-Time. *Sensors* **2021**, *21*, 2440.
- (38) Reyes-Romero, D.; Behrmann, O.; Dame, G.; Urban, G. Dynamic Thermal Sensor for Biofilm Monitoring. *Sensors and Actuators A: Physical* **2014**, *213*, 43–51.
- (39) Firstenberg-Eden, R.; Zindulis, J. Electrochemical Changes in Media due to Microbial Growth. *Journal of Microbiological Methods* **1984**, *2*, 103–115.

- (40) Lee, R. C. Cell Injury by Electric Forces. *Annals-New York Academy of Sciences* **2005**, *1066*, 85.
- (41) Taghian, T.; Narmoneva, D.; Kogan, A. Modulation of Cell Function by Electric Field: a High-Resolution Analysis. *Journal of the Royal Society Interface* **2015**, *12*, 20150153.
- (42) Funk, R. H.; Monsees, T. K. Effects of Electromagnetic Fields on Cells: Physiological and Therapeutical Approaches and Molecular Mechanisms of Interaction. *Cells Tissues Organs* **2006**, *182*, 59–78.
- (43) Watanabe, I.; Okada, S. Effects of Temperature on Growth Rate of Cultured Mammalian Cells (L5178Y). *The Journal of Cell Biology* **1967**, *32*, 309–323.
- (44) Shellman, Y. G.; Ribble, D.; Yi, M.; Pacheco, T.; Hensley, M.; Finch, D.; Kreith, F.; Mahajan, R. L.; Norris, D. A. Fast Response Temperature Measurement and Highly Reproducible Heating Methods for 96-Well Plates. *Biotechniques* **2004**, *36*, 968–976.
- (45) Kalamida, D.; Karagounis, I. V.; Mitrakas, A.; Kalamida, S.; Giatromanolaki, A.; Koukourakis, M. I. Fever-Range Hyperthermia vs. Hypothermia Effect on Cancer Cell Viability, Proliferation and HSP90 Expression. *PLoS One* **2015**, *10*, e0116021.
- (46) Zhao, P.; Jiang, H.; Su, D.; Feng, J.; Ma, S.; Zhu, X. Inhibition of Cell Proliferation by Mild Hyperthermia at 43 C With Paris Saponin I in the Lung Adenocarcinoma Cell Line PC-9. *Molecular Medicine Reports* **2015**, *11*, 327–332.
- (47) Chauhan, J.; Neelakantan, U. An Experimental Approach for Precise Temperature Measurement using Platinum RTD PT1000. 2016 International Conference on Electrical, Electronics, and Optimization Techniques (ICEEOT). 2016; pp 3213–3215.
- (48) *Drying Phenomena*; John Wiley & Sons, Ltd, 2015; pp 457–459.
- (49) 96-Well Plate Dimensions [Standard Microplate] (2014) [Online]. Available: <https://www.wellplate.com/96-well-plate-dimensions/>, retrieved on 2020/06/16.

- (50) ANSI/SLAS Microplate Standards (2012) [Online]. Available: <https://www.slas.org/education/ansi-slas-microplate-standards>, retrieved on 2020/06/16.
- (51) Thermtest. (2020) Materials Thermal Properties Database. [Online]. Available: <https://thermtest.com/materials-database>, retrieved on 2020/06/01.
- (52) Green, D. W.; Perry, R. H. *Perry's Chemical Engineers' Handbook*; 2008; pp 2–117.
- (53) Bertrand, G. L.; Millero, F. J.; Wu, C.-h.; Hepler, L. G. Thermochemical Investigations of the Water-Ethanol and Water-Methanol Solvent Systems. I. Heats of mixing, Heats of Solution, and Heats of Ionization of Water. *The Journal of Physical Chemistry* **1966**, *70*, 699–705.
- (54) Dellinger, J. H. *The Temperature Coefficient of Resistance of Copper*; US Government Printing Office, 1911; p 72.

TOC Graphic

